Ion acceleration and anomalous transport in the near wake of a plasma limiter

D. P. Sheehan,[a] J. Bowles,[b] and R. McWilliams
Department of Physics and Astronomy, University of California, Irvine, California 92717

(Received 26 February 1997; accepted 9 June 1997)

Ion acceleration and anomalous transport were studied experimentally in the near wake region of an electrically floating disk limiter immersed in two different types of collisionless, supersonically flowing, magnetized plasmas: the first initially quiescent, the second initially turbulent. Ion densities and velocity distributions were obtained using a nonperturbing laser induced fluorescence diagnostic. Large-amplitude, low-frequency turbulence was observed at the obstacle edge and in the wake. Rapid ion and electron configuration space transport and ion velocity space transport were observed. Configuration space and velocity space transport were similar for both quiescent and turbulent plasma-obstacle systems, suggesting that plasma-obstacle effects outweigh the effects of initial plasma turbulence levels. © *1997 American Institute of Physics.* [S1070-664X(97)02809-7]

I. INTRODUCTION

Anomalous particle losses in tokamaks and other fusion test devices driven by electrostatic and magnetic fluctuations are a serious impediment to achieving controlled fusion.[1–5] Confinement degradation due to fluctuations is seen across a broad spectrum of plasma devices. For example, experiments in the Texas Experimental Tokamak (TEXT) have demonstrated clear correlations between electrostatic fluctuations and particle and energy losses.[6,7] Edge electrostatic fluctuations have been correlated with significant particle losses in the Madison Symmetric Torus (MST).[8] Sensitive measurements of ion cross-field transport versus density fluctuation levels have been made in *Q*-machine plasmas[9] and in the Columbia Linear Machine.[10]

Low-frequency turbulence is a universal feature in tokamaks;[11,12] in particular, resistivity gradient driven turbulence and collisional density gradient driven turbulence are believed to drive transport in edge plasmas, while drift wave turbulence is believed to dominate anomalous core transport. Limiters should affect the edge velocity shear layer, which both theoretical and experimental studies show can have a strong influence on turbulence and transport. Edge plasma turbulence and plasma-limiter interactions are receiving increasing attention.[12–16] Evidence mounts that edge plasma turbulence plays a major role in ion confinement.[17–25] Limiter-generated turbulence may enhance impurity transport into core plasmas, thereby degrading reactor efficiency.[26]

In addition to fusion plasmas, plasma-limiter interactions bear on plasma probe operation,[27] microstructure resolution of substrates in semiconductor device manufacture, and on space plasmas. Plasma wakes have been observed around planets, natural and artificial satellites,[28–34] and they have been investigated in the vicinity of the U.S. Space Shuttle.[35]

The present experiment examines the filling of the near wake in the presence of large-amplitude, low-frequency ($f \leqslant 50$ kHz) turbulence generated near an obstacle as plasma flows around it. Two different plasmas are flowed past the obstacle, representing opposite extremes in the initial turbulence level of the ambient plasma; in other respects, the systems are similar. The first is a quiescent plasma [Q-machine, Ba^+/e^-, $(\delta n/n)_{\rm rms} \leqslant 0.001$], such that waves and instabilities (except very small amplitude drift waves) can be attributed to plasma-obstacle effects. The second plasma, a $Ba^+/SF_6^-/e^-$ plasma, naturally exhibits large-amplitude, low-frequency ($f \leqslant 20$ kHz) wave turbulence and large density fluctuations $[(\delta n/n)_{\rm rms} \geqslant 0.25]$ throughout the plasma.[36] By investigating opposite extremes in initial plasma turbulence, one may infer the relative importance of this ambient turbulence relative to other effects, namely, plasma-obstacle effects. In this experiment, we find that ion cross-field transport levels exceed standard theoretical predictions, and appear to be independent of initial plasma turbulence levels.

Integrated ion phase space density plots were constructed for both plasma-obstacle systems utilizing laser induced fluorescence (LIF) diagnostics on singly ionized barium ions described elsewhere.[37,38] Near wake ion energization resulted in a twofold increase in the average component of the ion kinetic energy density perpendicular to the magnetic field. Comparison of experimental and numerical simulation results indicate spatial cross-field ion transport is far greater than predictions from ion cyclotron motion around the obstacle, classical diffusion, or Dupree turbulence predictions.[39] The Ba^+/e^- and $Ba^+/SF_6^-/e^-$ plasmas displayed similar levels of spatial transport and ion acceleration, suggesting that the initial plasma turbulence level was not fundamental to the development of the near wake. On the contrary, evidence suggests that a combination of obstacle-generated, strong, low-frequency turbulence ($f \leqslant 50$ kHz) and electrostatic sheaths largely determine wake development. In this paper, ''turbulence'' will refer to the condition in which the plasma displays a broadband, incoherent wave spectrum. ''Fluctuations'' may refer either to electrostatic or density fluctuations.

For plasma flowing past an obstacle, three downstream

[a]Present address: Department of Physics, University of San Diego, San Diego, California 92110; Electronic mail: dsheehan@acusd.edu
[b]Present address: Plasma Physics Division, Naval Research Laboratory, Washington, D.C. 20375.

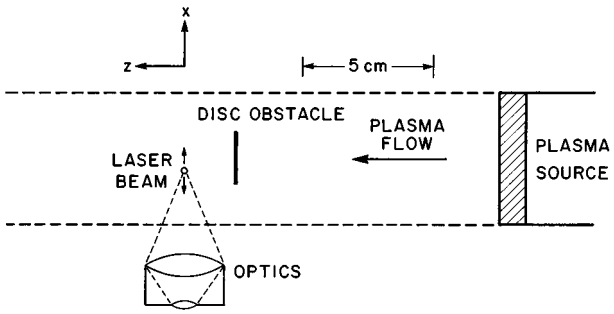

FIG. 1. Schematic of experimental plasma-obstacle system.

regions are distinguished: the near, middle, and far wakes.[40–46] The near wake, immediately downstream of the obstacle, consists of a void and a thin region of disturbed plasma at the interface of the void and ambient plasma. For an unmagnetized plasma, this boundary makes an angle $\theta = \tan^{-1}(1/M)$ with the plasma streaming vector, where M is the plasma Mach number, the ratio of plasma drift to thermal speeds. For this experiment, $M = v_D/c_s \sim 3$, where v_D is the plasma drift speed and c_s is the sound speed. Thus, the plasma flow is supersonic with respect to the obstacle. The middle wake, characterized by an ion flux peak[45,46] bridges the near and far wakes. In the far wake, the plasma makes its transition back to ambient plasma conditions. This experiment examines the near wake region.

Wakes in electron-free, negative ion plasmas (NIP) should be fundamentally different from those in electron–ion plasmas. Plasma space potentials should be reduced or absent in NIPs, since both plasma species should have comparable mobilities at a given temperature. As a result, effects of Debye screening of the obstacle also should be reduced or entirely absent. Given the residual electron densities in these experiments ($n_e/n_i \sim 0.05$), however, electrons still may affect expansion processes, owing to their greater thermal speeds. Expansion may be augmented in NIPs, however, by native turbulence.[36,47] In contrast to Q-machine electron–ion plasmas, which are free from substantial turbulence and which display essentially classical or near classical diffusion,[48] experimental NIPs may display strong turbulence $[(\delta n/n)_{\rm rms} \geqslant 1]$ and anomalous diffusion ($D_\perp \sim 10^4$ cm^2/s) (Refs. 36, 47, and 49).

II. METHODS

These experiments were performed in the U.C. Irvine Q machine.[50,51] The Q plasmas are cylindrical, steady state (length=1.2 m, diameter=5 cm, $n_i = n_e \sim 10^9$ cm^{-3}, $T_{e\parallel} \sim T_{e\perp} \sim T_{i\parallel} \sim T_{i\perp} \sim 0.2$ eV, $B = 3$ kG), and are produced by contact ionization of atomic barium ($m_{\rm Ba} = 137.3$ amu) vapor on an incandescently heated rhenium-coated tungsten disk hot plate (see Fig. 1). Here, $\perp$ and $\parallel$ refer, respectively, to the directions perpendicular and parallel to the confining magnetic field. Electrons thermionically emitted from the hot plate surface create a local sheath, which accelerates the contact-ionized Ba^+ ions to a drift velocity of roughly $v_d = 1.2\times10^5$ cm/s, or about three times the ion thermal velocity. This plasma, composed solely of a drifting Ba^+ 0.2 eV thermal population and a neutralizing 0.2 eV electron background population, is designated a Ba^+/e^- plasma in this text.

Undisturbed Q plasmas are very quiet (Q for ''quiescent''), possessing density fluctuations on the order of $(\delta n/n)_{\rm rms} \leqslant 0.001$. The central region of the plasma column, where the obstacle is located, is quiescent. The plasma beta value is roughly $\beta \sim 10^{-8} - 10^{-10}$.

The $Ba^+/SF_6^-/e^-$ plasma is produced from a Ba^+/e^- plasma by introducing gaseous SF_6 into the vacuum vessel at a pressure of $2-3\times10^{-5}$ Torr. Sulfur hexafluoride ($m_{\rm SF_6} = 146$ amu) is an electron scavenger with a large electron capture cross section for low-energy electrons, such as those found in Q machines. With SF_6, low residual electron densities ($n_e/n_i \sim 0.05$) can be achieved, accompanied by strong low-frequency turbulence ($f \leqslant 20$ kHz), and sizable plasma density fluctuations $[(\delta n/n)_{\rm rms} \sim 0.25]$. In fact, the turbulence level can be controlled by the partial pressure of SF_6.[47] At SF_6 pressures used in this experiment, the $Ba^+/SF_6^-/e^-$ plasma displays turbulence levels approximately 10^2-10^3 times greater than for the Ba^+/e^- plasma and density fluctuation levels roughly 10^2 times greater. The introduction of SF_6 also increases the drift velocity of the plasma from 1.2×10^5 cm/s to 1.7×10^5 cm/s. Also, the plasma floating and space potentials are driven to more positive values when the free electrons are depleted. For more details on NIPs, see Sheehan and co-workers.[36,38,47,49]

The density ratios of plasma species in the $Ba^+/SF_6^-/e^-$ plasma are roughly 1.0/0.95/0.05, respectively. Also, since SF_6 and Ba have virtually unity mass ratio ($m_{\rm SF_6}/m_{\rm Ba} = 1.06$) and almost unity particle density ratio, the SF_6^- and Ba^+ cyclotron and plasma frequencies are comparable [$\omega_{ci}(3\ {\rm kG}) = 2.1\times10^5$ rad/s, $\omega_{pi}(10^9\ {\rm cm}^{-3}) = 3.6\times10^6$ rad/s].

The floating potential, Φ_f, of a Q plasma is increased by the presence of SF_6. In a pure Ba^+/e^- plasma, $\Phi_f \sim -3$ V relative to the vacuum vessel ground. As SF_6 is introduced, Φ_f increases, approaching zero volts as the partial pressure of SF_6 reaches $P_{\rm SF_6} \sim 2-3\times10^{-5}$ Torr. This is expected since barium and sulfur hexafluoride masses and particle densities are comparable. No direct measurements of SF_6^- temperature were made, but, they are expected to be less than or comparable to electron and ion temperatures because of particle–particle and wave–particle collisions upstream from the diagnostic region. Because of their rough symmetries in mass, density, and, presumably, temperature, one expects the floating potential to be roughly zero based on von Neumann's symmetry principle; this is supported by measurements of Φ_f in $Ba^+/WF_6^-/e^-$ plasmas.[36] If $\Phi_f = 0$, one expects plasma sheaths around the obstacle to be reduced in strength, or absent. Ion acceleration by plasma sheaths around obstacles in a plasma with a nonzero floating potential has been studied.[52]

Barium is used because of the convenient electronic properties of the Ba^+ ion, allowing the use of LIF as a diagnostic. Laser induced fluorescence techniques[53–55] are used to measure ion velocity distributions. A single frequency laser beam (ω_L, k_L) excites optical transitions in barium ions, which are measured by collection apparatus exterior to the

plasma. This diagnostic is nonperturbing to the plasma, possesses good spatial, velocity, and temporal resolutions (1 mm^3, 3×10^3 cm/s, and 1 μs, respectively). Ion velocity selection occurs according to the Doppler relation

$$\omega_L - k_L \cdot v_i = \omega_0, \tag{1}$$

where ω_0 is the natural Ba^+ transition frequency. As indicated by Eq. (1), velocity components along the axes perpendicular to k_L are not preferentially selected. Thus, for example, the measured distribution is

$$f_i(x,v_y,t) = \int\int f_i(x,v,t)\,dv_x dv_z, \tag{2}$$

for a laser beam in the y direction.

The experimental obstacle (see Fig. 1) consisted of an electrically floating tantalum disk (diameter=1.9 cm, thickness=0.75 mm) supported by a thin 304 stainless-steel wire (diameter=0.5 mm) centered in the plasma column with the disk surface-normal vector parallel to the supersonic plasma flow. The ratio of the Larmor radius, ρ_i, to the obstacle radius, d, was $\rho_i/d \simeq 0.2$. For discussion, the axial coordinate, z, is in the direction of the imposed magnetic field and plasma drift velocity. The origin of coordinates is taken to be the disk edge, such that the discrete ion velocity distributions are taken along the x axis at various points in the direction of the disk's diametrical chord. The y axis is perpendicular to x, tangential to the plane of the disk, and aligned with the direction of laser beam propagation. Time scales for wake phenomena were estimated from values of axial position downstream of the obstacle, z, assuming a constant plasma drift velocity, v_d, through the relation, $t = z/v_d$. In this sense, the drifting plasma acted as a streak camera.

Spatially resolved phase-space reconstructions of this system were obtained from a series of discrete ion velocity distributions, $f(x,y,v_y)$, taken at 1–2 mm intervals along the x axis at various axial (z) locations, as described elsewhere.[37,38] In addition, frequency spectra ($0\ \mathrm{Hz} \leqslant f \sim 4 f_{pi} \leqslant 8$ MHz) were obtained by rf probes at the locations of the LIF scans. It is noted that, unlike the LIF diagnostic, the rf probe diagnostic physically perturbed the plasma and may have altered the particle dynamics and wave activity nearby.

In order to discriminate between plasma effects and individual ion cyclotron motion into the near wake, a numerical simulation was performed to model magnetized ion trajectories around the obstacle, similar to Schmitt,[43] and Waldes and Marshall.[44] The present model incorporates only ion thermal, drift, and cyclotron motions and does not include self-consistent electric fields and particle diffusion, as do more sophisticated models.

III. RESULTS

Ions in the near wake of the disk obstacle for both experimental configurations, initially quiescent or initially turbulent plasmas, displayed significant and comparable configuration space and velocity space transport. Figures 2(a)–2(c) display $x - v_y$ phase-space density plots for the $Ba^+/SF_6^-/e^-$ plasma-obstacle system at three axially sequential locations: $z=0.4$, 0.9, and 1.4 cm. (Since Ba^+/e^- and $Ba^+/SF_6^-/e^-$ results are similar, it suffices to display the latter.) Phase-space density plots were constructed from multiple individual velocity distributions, $f(x,v_y)$, taken along radial chords (x direction) in the wake of the obstacle at fixed axial (z) locations. Velocity distributions were digitized with the y velocities ascertained corresponding to 5%, 10%, 15%, 20%, 30%,..., of the maximum phase-space density. (This maximum is the $v_y=0$ phase-space density in the unperturbed plasma away from the obstacle.) Points of constant phase-space density at multiple x locations were smoothly connected to generate phase-space plots, as in Fig. 2.

The numerical phase-space plots, Fig. 2′, were generated similarly to the experimental plots. The plasma was modeled as an axially drifting bi-Maxwellian and the obstacle as an infinite half-plane of zero thickness. [Since the disk radius substantially exceeded the thermal ion gyroradius ($R_D/\rho_i > 5$), the half-plane approximation was reasonable.] The numerical velocity distribution, $f(v_y)$, at a target point in the wake was built up from the contributions from a field of source points upstream of the obstacle. The v_y component contributed by each source point to the target was established geometrically. The statistical weight of each source point was the product of three weighting factors: the first representing the source plasma ion velocity distribution, accounting for the radial separation of the source and target; the second accounted for the transmission probability of particles past the obstacle; and the third accounted for the axial distance of the target from the obstacle, considering the gyrophase of the ions. The contributions of all source points in the upstream field were summed to establish $f(v_y)$ at a target point (x,z). Convergence of this discrete sum to the continuum limit was checked by varying the number of source points from 100 to 2500; when normalized, each gave identical $f(v_y)$'s.

The axial separation between experimental plots, $\Delta z \simeq 0.5$ cm, corresponds to temporal separations of $\Delta t \simeq 3\times10^{-6}$ s, assuming the plasma drift velocity remains constant. LIF measurements of the free-flowing NIP indicate its drift velocity was roughly 1.7×10^3 m/s. Experimental and numerical simulation diagrams are presented together for comparison, the experimental [Figs. 2(a)–2(c)] on the left, the numerical simulation [Figs. 2(a′)–2(c′)] on the right. The diagrams presented span one velocity and one configuration space dimension on which contours of constant phase-space density are plotted, much as contours of constant elevation are plotted on topographical maps. The contours represent percentages of the maximum phase-space density in the ambient plasma. In order to interpret the plots, it may be useful to examine the coordinate system in Fig. 1. In this experiment, $x=0$, $z=0$ is the location of the edge of the disk; $z<0$ is upstream; $x<0$ is in the wake, while $x>0$ is radially outside the wake.

The right-hand side of each experimental and simulated plot ($x \geqslant 2$ mm), representing the ambient plasma, consists of roughly parallel contours of phase-space density of a generally Maxwellian nature. Behind, and radially near the obstacle (i.e., within a Larmor radius of the obstacle edge), phase-space density distortions result as plasma enters the

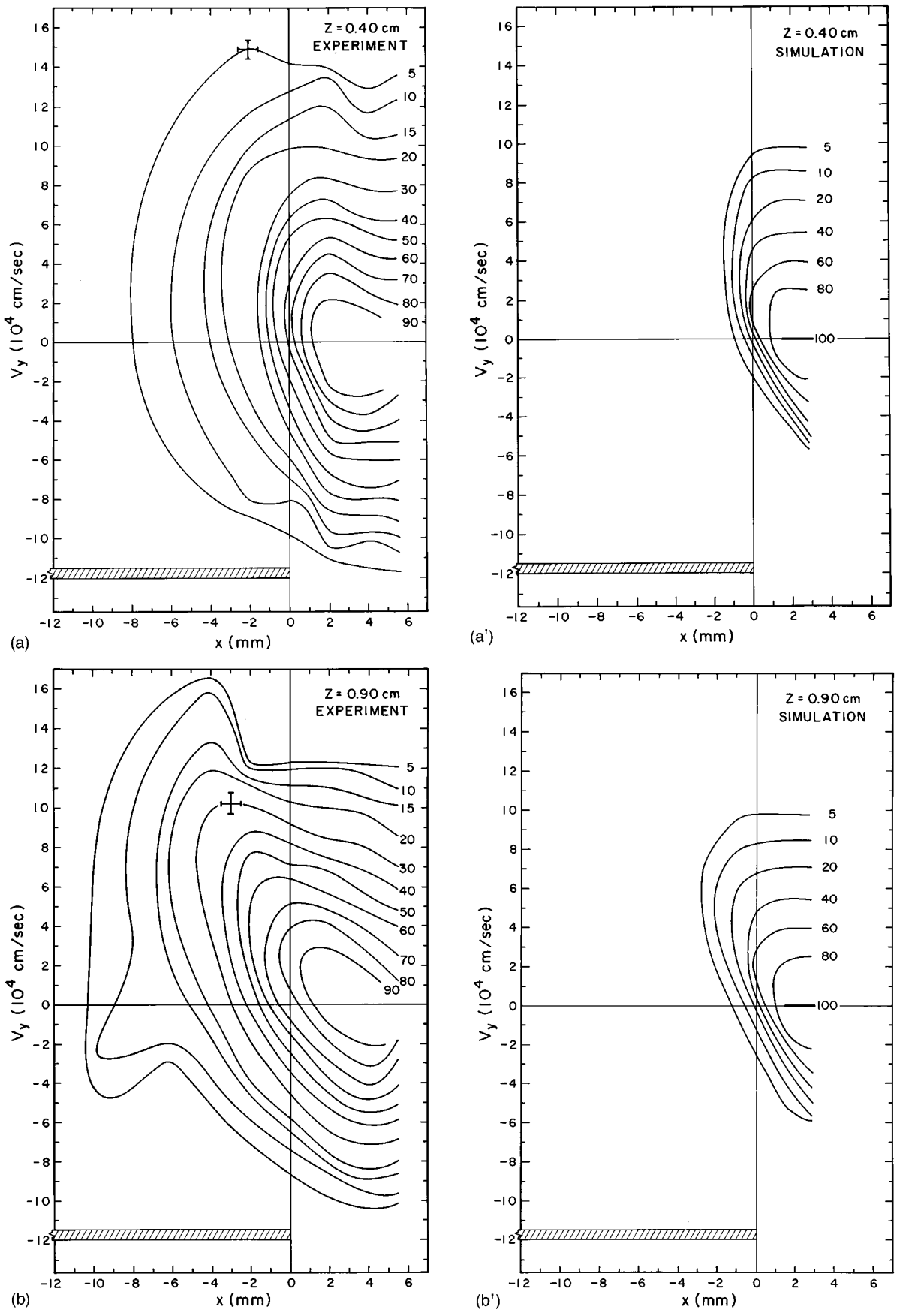

FIG. 2. Experimental phase-space density plots of the near wake of initially turbulent plasma ($n_i = 7 \times 10^8$ cm^{-3}, $B = 3$ kG) at various axial locations (a: 0.40 cm, b: 0.90 cm, c: 1.40 cm). (a′–c′): Phase-space density plots of simulated ion cyclotron motion into the near wake. Horizontal bar indicates obstacle radial location. Initially quiescent plasma rendered similar results.

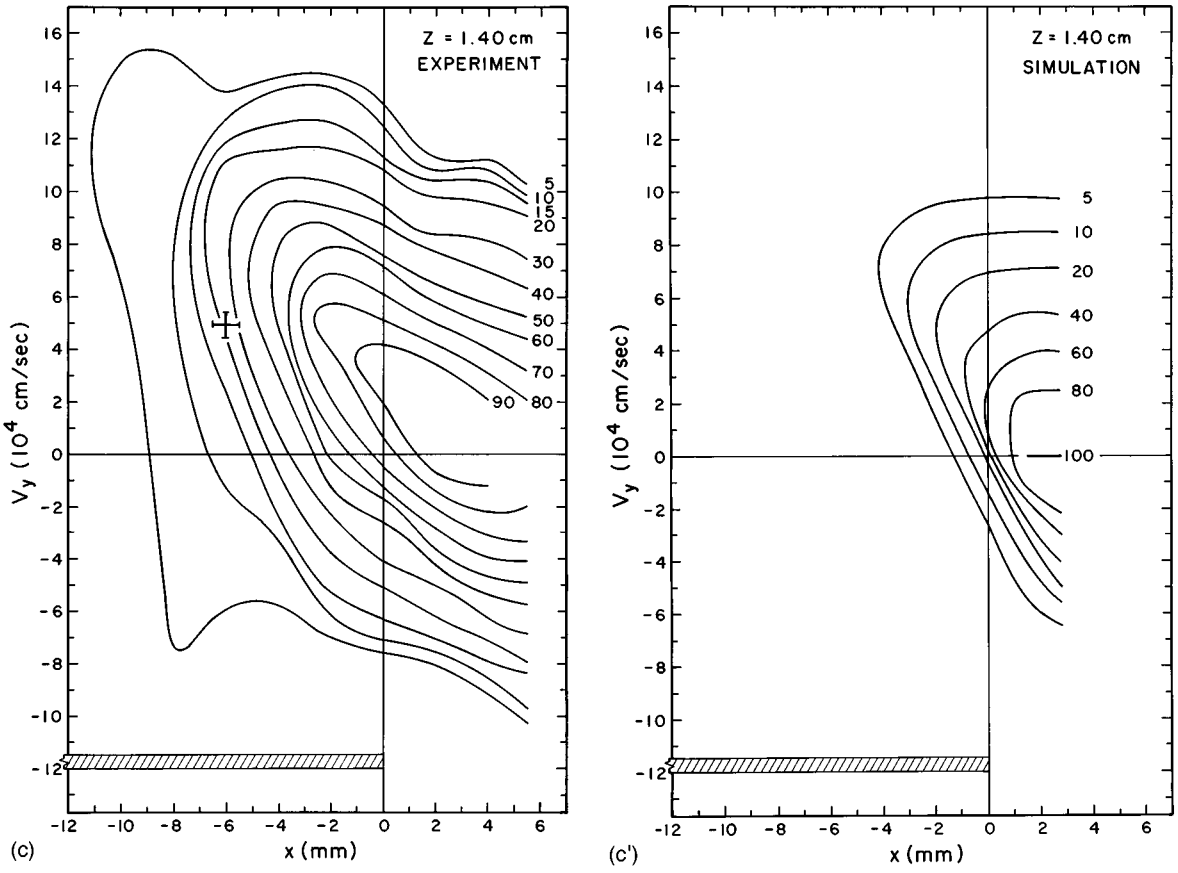

FIG. 2. (*Continued.*)

void downstream of the obstacle. Both experimental and numerical diagrams exhibit contours preferentially reaching into the positive v_y-negative x quadrant of phase space, forming nested ''ears'' of phase-space density. This is caused by the predominant $+v_y$ motions of barium ions as they spiral behind the obstacle into the void. At $z=1.4$ cm, ''ear lobes'' are present in the $-v_y$ half plane. These are consistent with $-v_y$ ions spiraling in from the other side of the obstacle. (Note that the obstacle extends to $x=-20$ mm.) Experimental contours extend further into the void than simulation contours, indicating greater ion configuration space transport than can be accounted for solely by cyclotron motion. Also, ion velocity space transport is evident in the form of high $+v_y$ ions, particularly in the 20%, 15%, 10%, and 5% contours, but also in the higher percentage contours for axial locations further downstream of the obstacle. Experimental contours not only extend more deeply radially behind the obstacle than simulation contours, but also higher vertically along the $+v_y$ axis, forming ''Vulcan pointy ears'' of phase-space density. Physically, this indicates ion acceleration perpendicular to the magnetic field. From this, one may infer the presence of electric fields.

As noted previously, the Ba^+/e^- and $Ba^+/SF_6{}^-/e^-$ plasmas differed by orders of magnitude in their electrostatic turbulence and density fluctuation levels, and yet both plasmas displayed similar degrees of ion configuration space and velocity space transport, suggesting that the initial level of

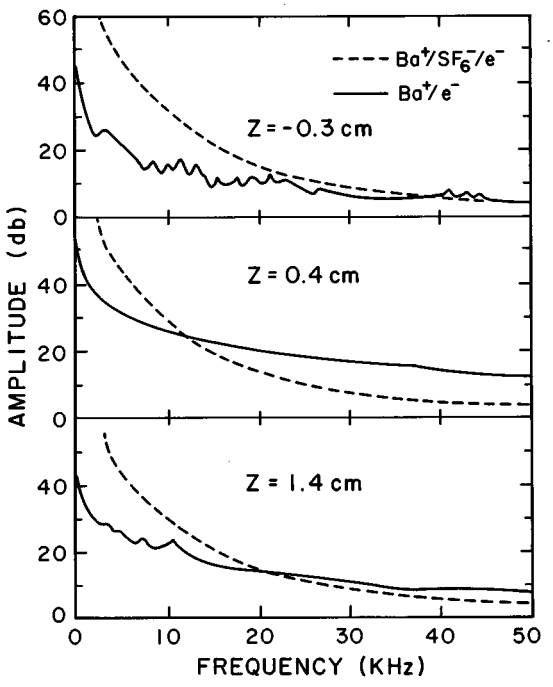

FIG. 3. Wave spectra for initially quiescent plasma [Ba^+/e^- (—)], and initially turbulent plasma [$Ba^+/SF_6{}^-/e^-$ (-·-·-·)] at three axial locations along plasma flowing vector tangential to obstacle edge. Wave turbulence increases as plasma passes the obstacle.

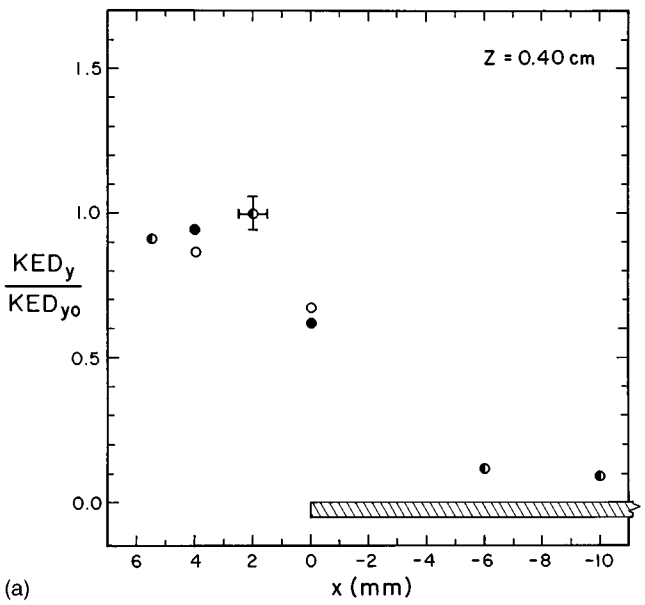

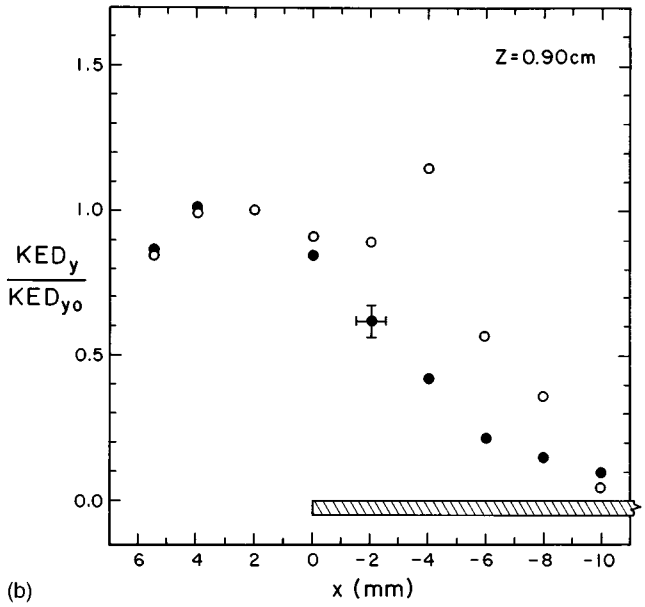

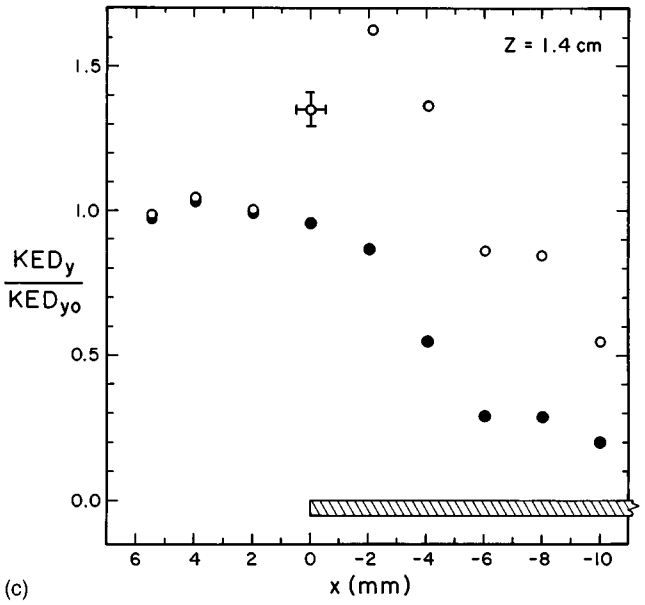

FIG. 4. (a)–(c) Normalized y component of ion kinetic energy density ($\mathrm{KED}_y/\mathrm{KED}_{yo}$) for turbulent plasma near wake at various axial locations, ● KED_y for thermal ions, theoretical, and ○ KED_y for experimental ions.

plasma turbulence is not fundamental to wake filling; rather, this evidence indicates that obstacle-generated turbulence and, possibly, static electric fields are decisive factors.

Wave spectra ($0 \leqslant f \leqslant 8$ MHz$\sim 4f_{pi}$) were obtained at various axial and radial locations downstream of the obstacle in both plasma types. In the Ba^+/e^- plasma, large-amplitude, low-frequency, broadband noise ($0 \leqslant f \leqslant 50$ kHz) was enhanced particularly in the vicinity of the obstacle edge where intensity increases up to 15 dB over ambient plasma levels were recorded. The $Ba^+/SF_6^-/e^-$ plasma showed only small increases in turbulence, at most about 5 dB over ambient conditions. Higher frequency waves ($f \geqslant 100$ kHz) were not seen. In Fig. 3, wave spectra for Ba^+/e^- and $Ba^+/SF_6^-/e^-$ plasmas are presented for three representative axial positions along the line of the plasma flowing vector past the obstacle edge ($x=0$, $y=0$). Note, for the Ba^+/e^- plasma, the noise level increases significantly (~ 15 dB) as the plasma passes the obstacle.

Ion kinetic energy densities (KED_y) in the near wake increased nearly a factor of 2 over ambient plasma values. In Figs. 4(a)–4(c), experimental and theoretical ion kinetic energy densities ($\mathrm{KED}_y/\mathrm{KED}_{yo}$) are presented for a series of axial locations in the near wake. Here, KED_{yo} is the y component of kinetic energy density for thermal (0.34 eV), ambient plasma ions not affected by the obstacle or wake regions. Experimental curves were generated from $mv_y^2/2$ moment integrations of the phase-space plots in Fig. 2. Radially inside the obstacle, immediately behind the obstacle ($z=0.4$ cm), the experimental KED_y coincides well with the KED_y predicted for purely ambient thermal ions, but further downstream, kinetic energy densities progressively increase beyond thermal levels. Radially outside the obstacle ($x \geqslant 0.0$ cm), experimental and theoretical values coincide well at all axial locations. The increase in KED_y radially inside the obstacle is attributed to ion acceleration by near wake electric fields. Preferential entry of high $v_\perp$ ions into the wake is not a plausible mechanism since it would result in

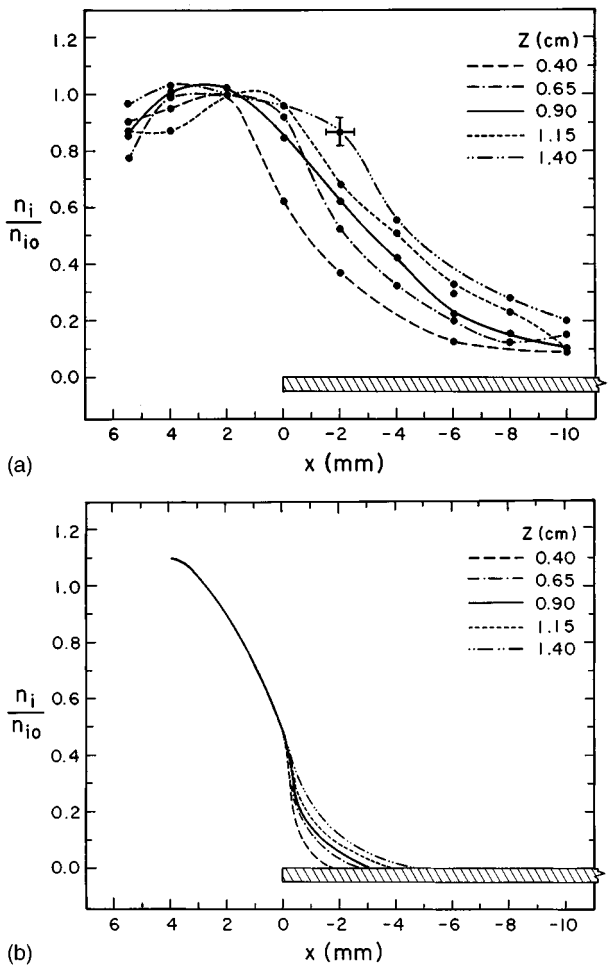

FIG. 5. Normalized ion density (n_i/n_{io}) in the near wake. (a): experiment, and (b): simulation.

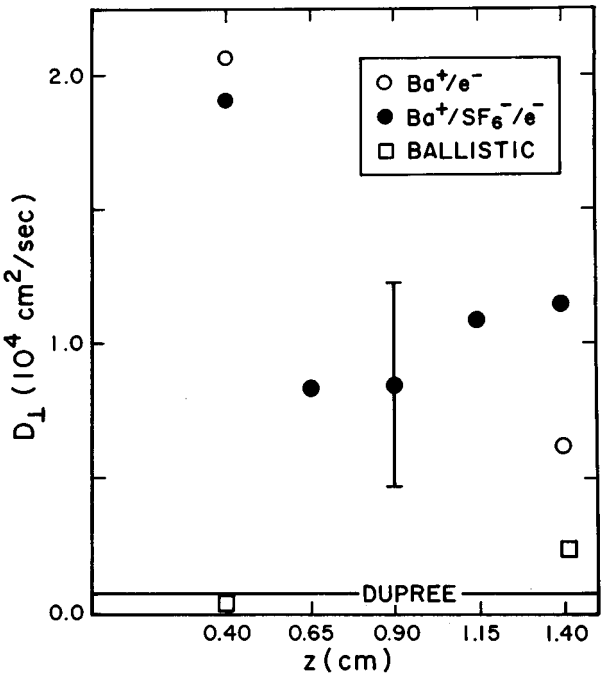

FIG. 6. Ion transport coefficient, $D_\perp$, versus axial distance in the wake, z, for initially quiescent (○), and initially turbulent (●) plasmas, simulated ion cyclotron motion (□), and Dupree predicted turbulent diffusion (solid line) for density fluctuation level, $(\delta n/n)_{\rm rms}\sim 0.25$.

depletion of high $v_\perp$ ions in the ambient plasma, which was not observed.

This ion acceleration shares simularities with other observations. For example, Hairapetian and Stenzel[56] observed ion acceleration to energies above tail electron energies when a two-electron-population argon ion plasma expanded into a vacuum. Ion acceleration was attributed to a potential double layer, which arose from the separation of the bulk and tail electron populations. Although their system is substantially different from the present experiment, for instance, their ion acceleration occurred parallel, rather than perpendicular, to the magnetic field, theirs involved a transient, traveling sheath, rather than a steady-state process as with ours; and theirs did not involve an obstacle, it did show that, in principle, ions can be accelerated above thermal energies by native plasma processes.

Rapid cross-field ion transport of similar degree was seen in the near wake of both plasma types. Radial, normalized barium ion density profiles are presented in Fig. 5(a) for several axial locations in $Ba^+/SF_6^-/e^-$. For comparison, radial density profiles from simulated quiescent plasma ion cyclotron motion are presented in Fig. 5(b). Clearly, experimental ion transport exceeds transport from ion cyclotron motion alone. For both the initially quiescent and initially turbulent plasmas, roughly half of the configuration space transport occurs within 0.4 cm of the obstacle, with the remainder occurring over the following 1 cm. Density profiles further downstream out to $z=5.4$ cm indicated less additional transport. This may be due to the relaxation of edge density gradients, sheaths, and turbulence, which can drive transport.

For the following discussion, ion transport will be quantified in terms of a formal transport coefficient, $D_\perp$,

$$D_\perp=\frac{1}{2}\frac{\delta\langle x^2\rangle}{t}, \tag{3}$$

where

$$\langle x^2\rangle=\int n_i(x)x^2dx \Big/ \int n_i(x)dx, \tag{4}$$

and t is the time scale for transport, i.e., the plasma drift time to the axial location downstream. No attempt is made here to distinguish between diffusive transport, convection, or any other transport process; $D_\perp$ is formal in the sense that it simply quantifies the bulk cross-field displacement of ions. In Fig. 6, $D_\perp$ is plotted versus axial distance, z, from the obstacle for both quiescent and turbulent plasma. These data were inferred from experimental curves in Fig. 5(a). Included, for perspective, are $D_\perp$ assuming ions in cyclotron orbits (assuming a formal $D_\perp$ even though this is not a diffusive process) and for transport from Dupree.[39] It is assumed that density fluctuations are $(\delta n/n)_{\rm rms}\sim 0.25$, as were measured in the ambient $Ba^+/SF_6^-/e^-$ turbulent plasma. Classical $(1/B^2)$ diffusion rendered $D_\perp\sim 100$ cm^2/s. Several features are noteworthy. First, $D_\perp$ was similar for both ini-

tially quiescent and turbulent plasmas, indicating that the initial level of plasma turbulence was not decisive, but, rather, that plasma-obstacle effects were dominant. In fact, the location of maximum transport coincided with the location of strongest wave turbulence. Second, experimental $D_\perp$ values exceed Dupree's predictions, cyclotron motion, and classical collisional values. Third, $D_\perp$ initially decreases with distance from the obstacle, then stabilizes at a large value ($D_\perp \sim 10^4$ cm^2/s), suggesting the presence of locally strong transport processes for $z \leqslant 0.4$ cm, followed by strong and reasonably constant transport processes for $0.4\ \text{cm} \leqslant z \leqslant 2.4$ cm.

Electron transport coefficients [$D_\perp$(electron) $\sim 10^4$ cm^2/s] in the near wake, estimated from Langmuir probe electron flux measurements, were comparable to ion coefficients for both initially quiescent and initially turbulent plasmas.[49] Again, as for the rf probe measurements and unlike the LIF measurements, the Langmuir probe physically perturbed the plasma.

IV. DISCUSSION

Ion acceleration and transport described thus far are consistent with turbulent wave–particle interactions and electrostatic sheaths in the vicinity of the obstacle. Wake filling due to classical diffusion or particle cyclotron motion are untenable here, since they predict ion and electron transport coefficients far below experimental values. The cyclotron mechanism also fails since it predicts filling for only a limited distance within the disk edge; this distance is smaller than that which is observed experimentally. Explicitly, one has $D_\perp$(Experimental)$\sim 10^4$ cm^2/s for experimentally inferred transport, $D_\perp$(Classical)$\sim 10^2$ cm^2/s for predicted classical diffusion, and a ''formal'' $D_\perp$(Cyclotron)$\sim 10^3$ cm^2/s for wake filling due to ion cyclotron motion. Again, $D_\perp$ is ''formal'' in the sense that it describes bulk cross-field ion transport without specifying mechanism.

Self-similar plasma expansion processes also do not adequately explain near wake ion and electron transport and ion acceleration. The magnetized nature of the plasma is the fundamental impediment to the expansion description. First, by its cyclotron motion in either plasma, Ba^+ is expected to precede the negative species into the void either because of superior thermal speed or a larger Lamor radius. Consequently, a positive space-charge potential should develop in the wake. This should inhibit ion transport and decelerate ions; instead, the opposite effects were seen experimentally. Second, the observed cross-field transport of magnetized electrons cannot be explained by simple plasma expansion. For this experiment, by symmetry, electric fields developed by plasma expansion should be radial or longitudinal, but not azimuthal. Electrons, constrained to $E\times B$ drift, cannot migrate radially except in the presence of azimuthal fields, such as those produced by drift waves or other instabilities. Finally, simple plasma expansion does not account for enhanced near wake wave fields.

Some experimental results are consistent with electrostatic sheaths, others not. An obstacle in the Ba^+/e^- plasma should float negatively ($\Phi_f \sim -3$ V, here) and could scatter and accelerate ions into the wake via a negative sheath potential. However, the $Ba^+/SF_6^-/e^-$ plasma would have a much more positive floating potential due to its dearth of electrons and, therefore, would be expected to display less, rather than the observed comparable levels, of ion energization and cross-field transport. (Still, the 5% residual electron population, by virtue of its much greater thermal velocity, should affect plasma dynamics, and so, could foster sheaths. As a rule of thumb, electrons in NIPs become unimportant when the electron–ion density ratio falls significantly below the ion–electron thermal velocity ratio. This condition is not met in the present plasma so electrons should be taken into account.)

Ion flux peaks[45,46,52] were observed intermittently in the midwake region of this system several gyrolengths (10.5–11.1 cm) downstream in the Ba^+/e^- plasma at magnetic-field strengths of 4 and 6 kG (but not at 2 kG). Peaks were noisy and not reproducible in shape or magnitude. (Their fickleness is believed due, in part, to the perturbations by the Langmuir probe diagnostic.) Ion flux peaks have been observed in unmagnetized and partially magnetized plasmas.[45,46,52] They are believed to result from electrostatic ion focusing by fields associated with the obstacle. As described by Taylor,[57] two types of electric fields may arise around electrically floating obstacles in an unmagnetized plasma: (1) a negative Debye sheath of scale length λ_D, and (2) a negative potential gradient due to the difference in thermal velocities between electrons and ions. The Debye sheath is well understood. Wake potential gradients have been described theoretically by self-simular plasma expansion[58] and have been observed experimentally.[52] Unlike previous studies, ions in this system are magnetized ($\rho_i < R$). Although the Debye sheath remains, it is not understood how wake potentials evolve in these supersonically flowing, magnetized plasmas.

In and of themselves, the ion flux peaks are indicative of static potential structures around the obstacle, but several aspects of them are mysterious. First, given the strong wake turbulence, it is surprising that this well-defined structure can evolve several gyrolengths from the obstacle, since ions must maintain phase coherence over several gyroperiods in the presence of strong turbulence to form the peak. Second, the location of the peak is independent of magnetic-field strength (between 4 and 6 kG), even though the magnetic-field strength affects gyrolength, gyroradius, and, perhaps, even the wake turbulence levels. Third, the maximum of the flux peak lies approximately $4\rho_i$ (for thermal ions) radially inward from the obstacle edge. LIF measurements of the near wake do not indicate a coherent perpendicular energization of ions sufficient to account for this large ion flux $4\rho_i$ inward from the edge. This suggests ions must migrate coherently across field lines to coalesce into the peak. Rapid cross-field motion without energization is suggestive of turbulent transport, while the presence of the coherent peak structure suggests static electric fields. A comprehensive explanation for this midwake flux peak is not evident.

In the near wake, the observed transport of electrons and ions might be due to a combination of sheaths and turbulence. Evidence for sheaths has been discussed. For discussion of turbulence effects, let us review particle dynamics in the plasma-obstacle system. Over the axial distance investi-

gated in the near wake, ions act as if unmagnetized, therefore, they behave ballistically with respect to electric fields, rather than displaying significant $E\times B$ drift. Electrons, however, are highly magnetized and should display $E\times B$ drift. Also, this system is effectively collisionless for ion–ion collisions, and collisional for electron–electron collisions.

Large-amplitude, low-frequency, broadband noise was observed in the near wakes of both plasmas, particularly near the obstacle edge where diffusion was initiated. Drift wave electric field vectors, E_r and E_θ, are calculated to be of the proper orientation to account for the observed transport of both plasma species: radial for ions, and azimuthal for electrons. Drift waves fields possess wave vectors, which are primarily azimuthal and longitudinal, with wave numbers and electric fields and, typically, satisfy the relation[59–61]

$$E_r \sim E_\theta \gg E_z . \tag{5}$$

Positive and negative ions may diffuse via turbulent E_r and electrons $E\times B$ drift via E_θ.

One may estimate the strength of the turbulent E_τ from ion transport coefficients, $D_\perp$, to be

$$E_r \sim \frac{m}{q}\left(\frac{2}{\tau}\right)^{3/2} D_\perp^{1/2} \sim 2.2 \text{ V/mm}, \tag{6}$$

where m, q, and τ are, respectively, ion mass, charge, and time scale for diffusion, i.e., the plasma drift time through the near wake ($\tau \sim 1.5\ \mu$s).

Now consider an electron, initially at rest, $E\times B$ drifting radially into the wake with velocity $v_r=(cE_\theta)/B$. The necessary $E\times B$ drift velocity can be estimated by dividing the obstacle scale length ($R\sim 1$ cm) by the plasma diffusion time, $\tau \sim 1.5\ \mu$s. Solving for E_θ, one obtains

$$E_\theta = \frac{Bv_\tau}{c} \sim 2 \text{ V/mm}. \tag{7}$$

Electric-field strengths $|E_r|$ and $|E_\theta|$ are similar, as expected from Eq. (5).

Measurements of changes in near wake kinetic energy densities are explained by relatively modest electric fields, well below those calculated above. From Fig. 4(c), the y component of the kinetic energy density roughly doubled over thermal values; therefore, the average ion energy increased 0.34 eV. Since this energy was deposited within 0.5 cm of the disk edge, the average electric field necessary for ion energization may be estimated to be 0.34 V/0.5 cm$\sim$70 mV/mm.

If one ascribes the ion energization to wave fields, then these data suggest that $e\delta\Phi/kT > (\delta n/n)_{\text{rms}}$ and that $e\delta\Phi/kT \geqslant 1$. Other experiments have recorded similar results.[7,16,62,63] For example, in their measurements of space potential and low-frequency density fluctuations in the Impurity Study Experiment-B (ISX-B), Hallock *et al.*[62] observed $e\delta\Phi/kT_e \sim 2.5\text{–}30\,\delta n/n$ for $(\delta n/n)_{\text{rms}} \sim 0.07$ in the edge plasma behind a limiter. The edge plasma-limiter system of a tokamak constitutes a plasma-obstacle system. If one linearly extrapolates their results [$(\delta n/n)_{\text{rms}} \sim 0.07$] to the present experiment [$(\delta n/n)_{\text{rms}} \sim 0.25$] for transport scale lengths, 1–1.5 mm, one obtains electric fields of $E_\tau \sim 1$ V/mm, in rough agreement with previous estimates for drift waves [$E_\tau \sim 2$ V/mm, Eq. (7)]. Also, inferred ion transport coefficients from the ISX-B edge plasma are comparable to our experimental results, $D_\perp \sim 10^4$ cm^2/s. Wall erosion and surface sputtering can be sources plasma impurities. This experiment suggests that the near wake region of limiter-like structures could be enhanced sources of impurities. Not only is ion cross-field transport large here, but ion energies may be enhanced, thus, increasing erosion and sputtering yields.

The present experimental transport coefficients are an order of magnitude greater than those predicted by Dupree turbulence theory, however, they agree with independent experimental transport measurements.[9] There, $D_\perp$ was measured in Ba^+/e^- Q plasmas in the presence of broadband, low-frequency noise ($f \sim 50$ kHz$\sim f_{ci} \ll f_{pi}, f_{pe}, f_{ce}$) generated from parametric decay of antenna-launched lower hybrid waves into electrostatic ion cyclotron waves. A linear dependence of $D_\perp$ on $(\delta n/n)_{\text{rms}}$ was inferred experimentally for $0.002 \leqslant (\delta n/n)_{\text{rms}} \leqslant 0.04$ (see Fig. 7 in Ref. 9). Linear extrapolation of their results to the present experimental regime [$(\delta n/n)_{\text{rms}} \sim 0.25$] predicts $D_\perp \sim 10^4$ cm^2/s, as was inferred from the present data.

In summary, we report observations of anomalous velocity and configuration space transport of ions in the near wake of a plasma limiter in supersonic plasma flow. Configuration space transport was greater than expected for cyclotron motion of ions behind the obstacle, classical, or Dupree diffusion. In addition, ions were observed to increase the perpendicular component of their kinetic energy roughly a factor of 2 in the near wake over ambient plasma levels. The observed ion energization and cross-field transport may be due to a combination of electrostatic sheaths and wave turbulence; the evidence for a single cause is inconclusive.

ACKNOWLEDGMENTS

The authors gratefully acknowledge useful discussions with Dr. N. Rynn, Dr. H. Böhmer, and Dr. William Thompson of the University of California, San Diego. The authors appreciate the engineering support provided by Mr. S. Roe and Mr. D. Parsons.

This work was supported by National Science Foundation Grant No. 94-19192, a Cottrell College Science Award of Research Corporation, and by a University of San Diego University Professorship Grant (1996-97).

[1] S. J. Zweben and R. J. Taylor, Nucl. Fusion **21**, 193 (1981).
[2] S. J. Zweben, P. C. Liewer, and R. W. Gould, J. Nucl. Mater. **111-112**, 39 (1982).
[3] S. J. Levinson, J. J. Beall, E. J. Powers, and R. D. Bengtson, Nucl. Fusion **24**, 527 (1984).
[4] A. J. Wootton, J. Austin, R. D. Bengtson, J. A. Boedo, R. V. Bravenec, D. L. Brower, J. Y. Chen, G. Cima, P. H. Diamond, R. D. Durst, P. H. Edmonds, S. P. Fan, M. S. Foster, J. C. Forster, R. Gandy, K. W. Gentle, R. L. Hickok, Y. X. Hey, S. K. Kim, Y. J. Kim, H. Lin, N. C. Luhmann, S. C. McCool, W. H. Miner, A. Ouroua, D. M. Patterson, W. A. Peebles, P. E. Phillips, B. Richards, C. P. Ritz, T. L. Rhodes, D. W. Ross, W. L. Rowan, P. M. Schoch, D. Sing, E. J. Synakowski, P. W. Terry, K. W. Wenzel, J. C. Wiley, X. Z. Yang, X. H. Yu, Z. Zhang, and S. B. Zheng, Plasma Phys. Control. Fusion **30**, 1479 (1988).
[5] B. A. Carreras, P. H. Diamond, M. Murakami, J. L. Dunlap, J. D. Bell, H. R. Hicks, J. A. Holmes, E. A. Lazarus, V. K. Pare, P. Similon, C. E. Thomas, and R. M. Wieland, Phys. Rev. Lett. **50**, 503 (1983).
[6] W. L. Rowan, C. C. Klepper, C. P. Ritz, R. D. Bengtson, K. W. Gentle, P.

E. Phillips, T. L. Rhodes, B. Richards, and A. J. Wootton, Nucl. Fusion **27**, 1105 (1987).
[7]C. P. Ritz, R. V. Bravenec, P. M. Schoch, R. D. Bengtson, J. A. Boedo, J. C. Forster, K. W. Gentle, Y. He, R. L. Hickok, Y. J. Kim, H. Lin, P. E. Phillips, T. L. Rhodes, W. L. Rowan, P. M. Valanju, and A. J. Wootton, Phys. Rev. Lett. **62**, 1844 (1989).
[8]T. D. Rempel, C. W. Spragins, S. C. Prager, S. Assadi, D. J. Den Hartog, and S. Hokin, Phys. Rev. Lett. **67**, 1438 (1991).
[9]R. McWilliams, M. K. Okubo, and N. S. Wolf, Phys. Fluids B **2**, 523 (1990).
[10]B. Song, A. K. Sen, and P. Tham, Phys. Fluids B **5**, 4341 (1993).
[11]P. C. Liewer, Nucl. Fusion **25**, 543 (1985).
[12]F. L. Hinton and R. D. Hazeltine, Rev. Mod. Phys. **48**, 239 (1976).
[13]R. H. Cohen and D. Ryutov, Comments Plasma Phys. Control. Fusion **16**, 255 (1995).
[14]S. J. Zweben, J. McChesney, and R. W. Gould, Nucl. Fusion **23**, 825 (1983).
[15]P. G. Weber, J. C. Ingraham, R. F. Ellis, G. A. Wurden, C. P. Munson, and J. N. Downing, Phys. Fluids B **3**, 1701 (1991).
[16]C. P. Ritz, D. L. Brower, T. L. Rhodes, R. D. Bengtson, S. J. Levinson, V. C. Luhmann, W. A. Peebles, and E. H. Powers, Nucl. Fusion **27**, 1125 (1987).
[17]A. V. Nedospasov, V. G. Petrov, and G. N. Fidel'man, Nucl. Fusion **25**, 21 (1985).
[18]L. S. Scaturro and B. Kusse, Nucl. Fusion **18**, 1717 (1978).
[19]K. F. Alexander, K. Gunther, W. Hintze, M. Laux, P. Pech, H.-D. Reiner, and A. V. Chankin, Nucl. Fusion **26**, 1575 (1986).
[20]Y. Shimomura, M. Keilhacker, K. Lackner, and H. Murmann, Nucl. Fusion **23**, 869 (1983).
[21]H. A. Claassen and H. Repp, Nucl. Fusion **21**, 589 (1981).
[22]H. Ohtsuka, M. Maeno, N. Suzuki, S. Donoshima, S. Yamamoto, and N. Ogiwara, Nucl. Fusion **22**, 823 (1982).
[23]Proceedings of the 4th Plasma Edge Theory in Fusion Devices, Varenna, Italy 1993, edited by R. Chodura and D. F. Düchs [Plasma Phys. **34** (1993–94)].
[24]S. K. Erents, S. Clement, P. J. Harbour, L. DeKock, G. M. McCracken, J. A. Tagle, and P. R. Thomas, J. Nucl. Mater. **176/177**, 301 (1990).
[25]A. LaBombard, A. A. Grossman, and R. W. Conn, J. Nucl. Mater. **176/177**, 548 (1990).
[26]V. Phillips, E. Vietzke, and M. Erdweg, J. Nucl. Mater. **162–164**, 550 (1989).
[27]G. F. Matthews, P. C. Stangeby, and P. Sewell, J. Nucl. Mater. **145–147**, 220 (1987).
[28]A. V. Gurevich and L. P. Pitaevsky, Prog. Aerosp. Sci. **16**, 227 (1975).
[29]C. L. Henderson and U. Samir, Planet. Space Sci. **15**, 1499 (1967).
[30]U. Samir and G. L. Wrenn, Planet. Space Sci. **20**, 899 (1972).
[31]U. Samir and E. G. Fontheim, Planet. Space Sci. **29**, 975 (1981).
[32]D. A. Gurnett, S. K. Scarf, and W. S. Kurth, J. Geophys. Res. **87**, 1395 (1982).
[33]D. S. Intrilagator and F. L. Scarf, Geophys. Res. Lett. **9**, 1325 (1982).
[34]J. D. Mihalov and A. Barnes, J. Geophys. Res. **87**, 9045 (1982).
[35]G. Murphy, J. Pickett, N. D'Angelo, and W. S. Kurth, Planet. Space Sci. **34**, 993 (1986).
[36]D. P. Sheehan and N. Rynn, Rev. Sci. Instrum. **59**, 1369 (1988).
[37]R. McWilliams and D. P. Sheehan, Phys. Rev. Lett. **56**, 2485 (1986).
[38]D. P. Sheehan, R. Koslover, and R. J. McWilliams, J. Geophys. Res. **96**, 14 107 (1991).
[39]T. H. Dupree, Phys. Fluids **10**, 1049 (1967).
[40]A. V. Gurevich, L. V. Paryiskaya, and L. P. Pitaevsky, Sov. Phys. JETP **22**, 449 (1966) (English translation).
[41]A. V. Gurevich, L. V. Paryiskaya, and L. P. Pitaevsky, Sov. Phys. JETP **27**, 476 (1968) (English translation).
[42]D. S. Intriligator and G. R. Steele, J. Geophys. Res. **87**, 6053 (1982).
[43]J. P. M. Schmitt, Plasma Phys. **15**, 677 (1973).
[44]J. Waldes and T. C. Marshall, Plasma Phys. **13**, 837 (1971).
[45]N. H. Stone, J. Plasma Phys. **26**, 351 (1981).
[46]N. H. Stone, J. Plasma Phys. **26**, 385 (1981).
[47]D. P. Sheehan, R. McWilliams, and N. Rynn, Phys. Fluids B **5**, 1523 (1992).
[48]R. McWilliams and M. Okubo, Phys. Fluids **30**, 2849 (1987).
[49]D. P. Sheehan, Ph.D. thesis, U.C. Irvine, 1987.
[50]N. Rynn and N. D'Angelo, Rev. Sci. Instrum. **31**, 1326 (1961).
[51]N. Rynn, Rev. Sci. Instrum. **35**, 40 (1964).
[52]R. L. Merlino and N. D'Angelo, J. Plasma Phys. **37**, 185 (1987).
[53]D. Dimock, E. Hinnov, and L. C. Johnson, Phys. Fluids **12**, 1730 (1969).
[54]D. N. Hill, S. Fornaca, and M. G. Wickham, Rev. Sci. Instrum. **54**, 309 (1983).
[55]R. A. Stern and J. A. Johnson, Phys. Rev. Lett. **34**, 1548 (1975).
[56]G. Hairapetian and R. L. Stenzel, Phys. Rev. Lett. **61**, 1607 (1988).
[57]J. C. Taylor, Planet. Space Sci. **22**, 121 (1974).
[58]U. Samir, K. H. Wright, and N. H. Stone, Rev. Geophys. Space Phys. **21**, 1631 (1983).
[59]H. W. Hendel, B. Coppi, F. Perkins, and P. A. Politzer, Phys. Rev. Lett. **18**, 439 (1967).
[60]H. W. Hendel, T. K. Chu, and P. A. Politzer, Phys. Fluids **11**, 2426 (1968).
[61]R. W. Motley, *Q-Machines* (Academic, New York, 1975).
[62]G. A. Hallock, A. J. Wootton, and R. L. Hickok, Phys. Rev. Lett. **59**, 1301 (1987).
[63]A. Lang and H. Boehmer, J. Geophys. Res. **88**, 5564 (1983).